Alkyl Chain Orientations in Dicyanomethylene-Substituted 2,5-Di(thiophen-2-yl)thieno-[3,2-b]thienoquinoid: Impact on Solid-State and Thin-Film Transistor Performance

Qinghe Wu, Shendong Ren, Mao Wang, Xiaolan Qiao, Hongxiang Li, Xike Gao, Xiaodi Yang, and Daoben Zhu**

A series of dicyanomethylene-substituted 2,5-di(thiophen-2-yl)thieno[3,2-b] thieno-quinoids, in which soluble alkyl chains (2-decyltetradecyls) are substituted at different positions (namely, 2,2′-positions (Compound 1); 3,3′-positions (Compound 2); 6,6′-positions (Compound 3)), are strategically designed and successfully synthesized. The photophysical and electrochemical properties as well as molecular packing of these new compounds are thoroughly investigated. Thin film transistor measurements reveal that Compounds 1–3 display markedly different charge transport performance. The solution processed thin film transistors of Compound 2 exhibits the highest electron mobility of up to 0.22 $cm^2 V^{-1} s^{-1}$ under ambient conditions, one and three orders of magnitude higher than those of Compounds 3 and 1, respectively, demonstrating the strong impact of alkyl chain orientations on transistor performance.

1. Introduction

To ensure the practical application of the low-cost and flexible organic field-effect transistors (OFETs) in displays, radio frequency identification (RFID) tags, and sensors, the organic semiconductors (OSCs) used in OFETs should be high-performance, stable, and solution-processable.[1] Two strategies are commonly used to design organic semiconductors with these properties. One is to develop a new type of π-conjugated core structure. Since the charge carriers are transported by hopping between adjacent molecules,[2] the carrier mobility is strongly affected by the π-conjugated cores.[3,4] The normal methods to develop new π-conjugated cores involve the modification of known conjugation cores through increasing conjugation length or expanding conjugation size,[5] introducing heteroatom substitutions,[6] and changing the symmetry of the molecular structures.[7] The other is introducing soluble side chains to a known π-conjugated core. The introduction of soluble side chains not only provides solution processing, but also changes the molecular packing in the solid state.[3,8,9] For example, side alkyl chains have been found to be interdigited between the adjacent backbone layers and resulted in short π–π stacking distance in solid states, which facilitate charge transport.[10] The requirement for the soluble side chains is that they should match the π-conjugated backbone to reach a compromise among solubility, efficient π–π stacking in solid state and formation of high quality thin films which are crucial for high performance OFETs.[11] By delicate modulation of soluble side chains to the known π-conjugated cores, many high performance OSCs have been synthesized. Currently, the impact of side chains with different length,[12,13] structure[14] and substituent density[10,15] on the molecular packing in solid state, film quality and device performance were deeply investigated and well understood. However, the influence of side chain orientations (the side chains are substituted on the different positions of a conjugated backbone), which would also strongly affect the performance of materials and be an efficient way to pursue excellent OSCs, does not attract much attentions.[16] We believe an in-depth investigation of how this aspect impacts on the molecular packing, film crystallinity, and device performance, would provide very useful information for the rational design of soluble, high-performance OSCs.

Though great progress has been made, compared with its p-type counterparts,[8,12,17] n-type OSCs still lag behind both in device performance (especially in terms of air stability) and

Q. Wu, Dr. S. Ren, M. Wang, Dr. X. Qiao, Prof. H. Li, Prof. X. Gao, Prof. D. Zhu
Shanghai Institute of Organic Chemistry
Chinese Academy of Sciences
Shanghai, 200032, China
E-mail: lhx@mail.sioc.ac.cn; zhudb@iccas.ac.cn
M. Wang
School of Materials Science and Engineering
East China University of Science and Technology
Shanghai, 200237, China
Dr. X. Yang
Laboratory of Advanced Materials
Fudan University
Shanghai, 200438, China
Prof. D. Zhu
Beijing National Laboratory for Molecular Sciences
Key Laboratory of Organic Solids
Institute of Chemistry
Chinese Academy of Sciences
Beijing, 100190, China

DOI: 10.1002/adfm.201202744

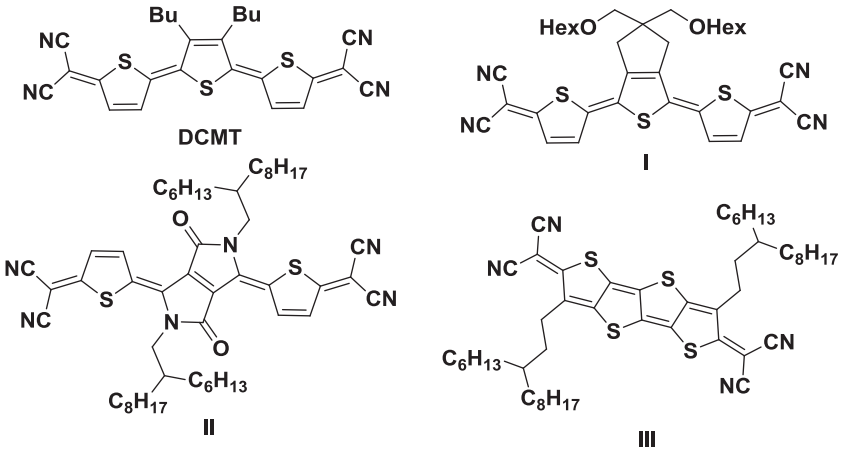

Scheme 1. The chemical structures of some typical thienoquinoidal-type OSCs.

in amounts and species of materials.[18] The lack of solution-processable, ambient-stable, and high-performance n-channel OSCs has become the bottle-neck for organic complementary circuits which require both n-channel and p-channel OSCs with comparable device performance.[19] As intensively investigated electron acceptors in charge-transfer complexes,[20,21] quinoidal compounds have established the reputation in the low-lying lowest unoccupied molecular orbital (LUMO) and strong electron affinity, which made them good candidates as ambient-stable n-channel OSCs.[22,23] Besides the low-lying LUMO, the quinoidal type semiconductors usually adopt face-to-face molecular stacking model and possess large packing coefficients in the solid state, which facilitated charge transport.[23,24]

Recently, the charge transport properties of dicyanomethylene-substituted quinoidal oligothiophenes have been studied. The vacuum deposited thin film transistors of **DCMT** (chemical structure given in **Scheme 1**) displayed an electron mobility of 0.2 $cm^2 V^{-1} s^{-1}$ under vacuum conditions.[25] Solution-processed thin films of **I** and **II** (chemical structures given in Scheme 1) exhibited electron mobilities of 0.16 and 0.35 $cm^2 V^{-1} s^{-1}$, respectively, under ambient conditions.[26] An electron mobility as high as 0.9 $cm^2 V^{-1} s^{-1}$ was observed for the drop-cast thin film transistors of **III** (chemical structure see Scheme 1) under ambient conditions without post treatment.[27] All of these results suggested quinoidal compounds were good candidates for ambient stable high performance n-channel OSCs. With the aim to explore the effect of side chain orientation on materials performance and the applications of quinoidal compounds in organic thin film transistors, dicyanomethylene-substituted 2,5-di(thiophen-2-yl)thieno[3,2-b] thienoquinoids with 2-decyltetradecyls substituents at different positions (the corresponding compounds are hereafter referred to a **1**, **2**, and **3**; see **Scheme 2**) were strategically designed and synthesized in this work. 2D grazing incidence X-ray diffraction (2D GIXD) results, thin film absorption spectra and thin film transistor characteristics showed the orientation of side alkyl chains strongly affected the molecular packing in solid states and transistor performance. An electron mobility as high as 0.22 $cm^2 V^{-1} s^{-1}$ was observed based on thin film transistors of **2** in ambient conditions, one and three orders of magnitude higher than those of compounds **3** and **1**.

2. Results and Discussion

2.1. Synthesis and Solubility

The synthetic route of compounds **1–3** is shown in Scheme 2. The preparation of thienoquinoid precursors **4–6** is described in the Supporting Information. Precursors **4–6** reacted with malononitrile in the presence of a base and Pd-catalyst and followed oxidization with saturated bromine to afford compounds **1–3** in moderate yields.[21] It should be noted that excessive bromine would destroy the green product to the dark-red byproduct and lower the yield. The chemical structures of all the compounds were characterized by nuclear magnetic resonance (NMR) spectroscopy, mass spectrometry (MS), high-resolution mass spectrometry (HRMS), and elementary analysis. Due to the long and branched side chains, compounds **1–3** displayed considerable solubility in common organic solvents such as tetrahydrofuran, dichloromethane, chloroform, 1,1,2,2-tetrochloroethane, chlorobenzene, and dichlorobenzene. However, their solubility differed greatly in the order **1** > **3** > **2** (**Table 1**). The melting points of compounds **1–3** also followed the same order as that of the solubility (Table 1). Considering the similar chemical structures of compounds **1–3** and the soluble nature of the alkyl chains, the variation of their solubility and melting points should be mainly determined by the intermolecular interactions in the solid state. The large difference of solubility and melting points of **1–3** suggests the strong impact of side alkyl chain orientation on their intermolecular interactions in the solid state.

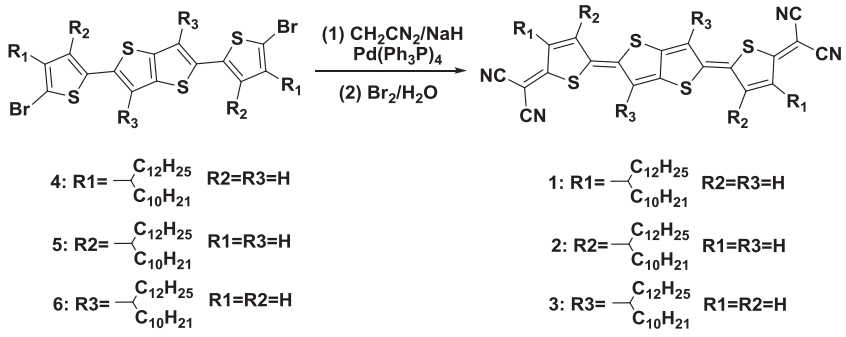

Scheme 2. Synthesis and chemical structures of dicyanomethylene-substituted 2,5-di(thiophen-2-yl)thieno[3,2-b] thienoquinoid derivatives **1–3**.

2.2. DFT MO Calculations

To better understand the impact of alkyl chain orientations on the HOMO and LUMO energy

Table 1. Solubilities, melting points, optical absorption data, electrochemical data, and theoretical calculation results of the OSCs **1**, **2**, and **3**.

Compd	Solubility [mg/mL][a)]	Melting point [°C]	λ_{max}^{sol} [nm]	λ_{max}^{film} [nm]	E_{red} [V][b)]	E_{ox} [V][b)]	LUMO [eV][c)]	HOMO [eV][d)]	E_g [eV]	LUMO [eV][e)]	HOMO [eV][e)]
1	40	138	710	674	−0.12	1.08	−4.32	−5.52	1.20	−4.16	−5.61
2	<25	231	705	605	−0.13	1.17	−4.31	−5.61	1.30	−4.19	−5.73
3	<40	163	720	720	−0.11	1.14	−4.33	−5.58	1.25	−4.26	−5.68

[a)]In $CHCl_3$; [b)]0.1 mol L^{-1} Bu_4NPF_6 in CH_2Cl_2 solutions with a scan rate of 50 mV s^{-1} and SCE as the reference; [c)]Estimated from $E_{LUMO} = -(E_{red} + 4.44)$; [d)]Estimated from $E_{HOMO} = -(E_{ox} + 4.44)$; [e)]Theoretical calculation results.

levels, the DFT MO calculations at the B3LYP-6-31 G(d) level of Gaussian 03 program were carried out to evaluate the frontier molecular orbital of compounds **1–3**. The long branched alkyl chains were replaced by isobutyl groups to reduce the calculation time and minimize the negative effect of the alkyl chain replacement. The π-conjugated backbone with no alkyl chain substituents (**DCM-DTTQ**) was also calculated for comparison (**Figure 1**). All the calculated compounds showed the same electron density distributions on HOMO and LUMO. In addition, the HOMO and LUMO energy levels of **1–3** (see Table 1) were shifted upward slightly compared with that of the **DCM-DTTQ** (HOMO: −5.85 eV; LUMO: −4.39 eV), which is ascribed to the weak electron-donating property of alkyl chains. The LUMO electron densities were fully delocalized across the whole conjugated core except the sulfur atoms, indicating that the alkyl substituents contributed equally to the LUMO energy levels. However, the distributions of HOMO electron densities were different on the 2,2′-, 3,3′- and 6,6′- positions, suggesting the alkyl chain orientations would affect the HOMO energy levels of **1–3**. No electrons in the HOMO orbital were localized in the 3,3′- positions, which resulted the lowest calculated HOMO energy levels of **2** and was consistent with the experimental result.

2.3. Electrochemical and Photophysical Properties

Cyclic voltammetry measurements were conducted to investigate the electrochemical properties of compounds **1–3**. Platinum electrodes were used as the working electrode and the counter electrode, and a saturated calomel electrode (SCE) was used as the reference electrode. The redox potentials were determined as the midpoints between peak potentials in the forward and reverse scan. As shown in **Figure 2**a, compounds **1–3** displayed one reversible reduction process and one reversible oxidative process in dichloromethane solution. The E^{red} of all compounds were more positive than −0.14 V and the LUMO/HOMO energy levels estimated from the CV were −4.32/−5.52, −4.31/−5.61, and −4.33/−5.58 eV for **1–3** respectively. The low LUMO energy level (lower than −4.0 eV) suggests the potential application of **1–3** as ambient-stable n-channel OSCs.[28] The HOMO energy levels of **2** was slightly lower than those of **1** and **3**, which was consistent with the trend obtained by DFT calculation. The HOMO-LUMO energy gaps calculated from CV were 1.20, 1.30, and 1.25 eV for **1–3**, respectively.

Figure 2b illustrates the solution and thin-film absorption spectra of **1–3**, and the optical data is shown in Table 1. The thin-films were prepared from the corresponding 20–30 mg/mL chloroform solution by spin coating at 2000 rpm for 20 s on a quartz glass substrate. The solution absorption spectra of **1–3** were nearly identical which indicated that the orientation of 2-decyltetradecyl substituents did not lead to fundamental changes or distortions of the π-conjugated backbone. The maximum absorption wavelength of the thin-film of **1** and **2** was blue shifted about 36 and 100 nm, respectively, while the absorption band of **3** become broader while the peak wavelength was unchanged compared with in solution, suggesting that **1–3** adopt different molecular packing in thin films.

Thermal annealing usually improves the order of molecules in the film and leads to higher transistor performance. The thin films of **1–3** were also treated by a thermal annealing technique (**Figure 3**). As depicted in Figure 3a, the thermally annealed thin film of **1** exhibited a large blue shift in comparison with that of the as-deposited film, which was caused by the molecule rearrangement in the annealing process. In remarkable contrast,

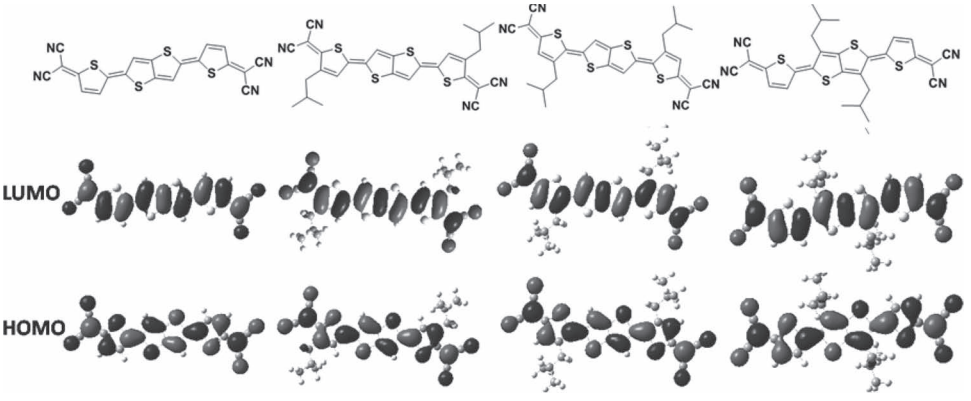

Figure 1. Calculated HOMO and LUMO of semiconductors **DCM-DTTQ**, **1**, **2**, and **3**.

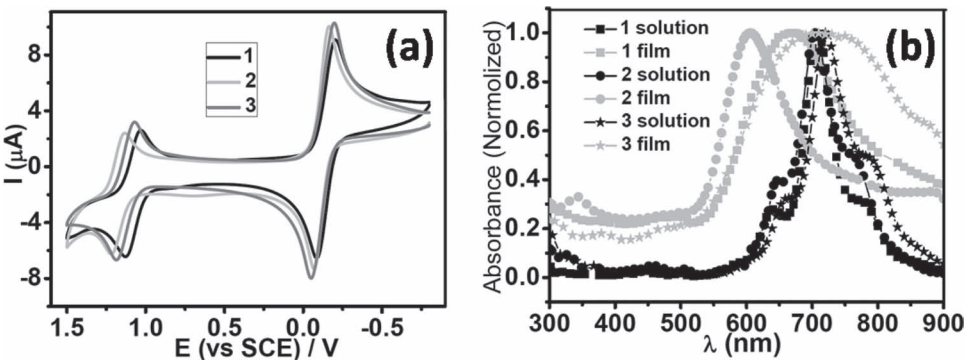

Figure 2. a) Cyclic voltammograms of **1**, **2**, and **3** (10^{-3} mol/L) with 0.1 mol/L Bu_4NPF_6 in CH_2Cl_2 solutions under scan rate of 50 mV s^{-1}; b) UV-vis absorption spectra of **1**, **2**, and **3** in dichloromethane solution (1×10^{-9} mol/L) and on a quartz substrate (as a deposited thin-film).

even annealed at 200 °C—slightly lower than the melting point (231 °C)—the thin films of **2** displayed identical absorption spectra, suggesting the molecular packing patterns in the as-deposited thin films were highly ordered and optimized. We assumed this was caused by the strong intermolecular interactions of **2**. Different from the H-type molecular aggregation of compounds **1** and **2** in the solid state, the thin films of **3** adopted J–type aggregation after annealing,[29] proved by the red shifted absorption compared with that of solution and the as-deposited thin film. The significant absorption differences of **1**–**3** thin films further confirmed that the alkyl chain orientation strongly affected the molecular packing in the thin films.

2.4. Thin-Film Microstructures and Morphologies

The atomic force microscopy (AFM) and X-ray diffraction (XRD) were employed to investigate the microstructures and morphologies of the thin films, which were correlated with the FET device performance (**Figure 4** and **Figure 5**). The quality of the as-deposited film of **1** was poor, as indicated by the weak peaks in the XRD scan and the featureless textures in the AFM images. Upon annealing the thin film at 80 and 120 °C, intensive sharp XRD peaks and successive reflections, which reached up to the the fifth order, were observed and plate-like textures were found in the AFM images. The lattice d-spacing determined from the reflection peaks was 34.40 Å.

The as-deposited thin films of **2** displayed multiple single family Bragg reflections, suggesting the high crystallinity of thin films. AFM images revealed that the as-deposited film of **2** was continuous and exhibited granular features. Thermal annealing the thin films at 80, 120, and 160 °C did not lead to more intensive peaks (in XRD) and not significantly enlarge the size of the grains (AFM images). These observations were consistent with the thin-film absorption spectra. The d-spacing calculated from the diffraction peaks was 33.20 Å, slightly shorter than that of **1**. Further increasing the annealing temperature to 200 °C, more elaborate diffraction peaks were clearly observed and large terrace-like crystalline grains with step height of 3.36 nm and size larger than 1 μm were formed. However, the grain boundary increased dramatically and the continuity of the film became worse.

For the thin films of **3**, the intensity of reflections was enhanced and the grain sizes were enlarged with the increase of thermal annealing temperature. Nevertheless, the crystallinity of thermal annealed films of **3** was significantly lower than that of **1** and **2**, since only two reflections were observed for **3** (thermal annealed 150 °C) and the reflections for **1** (thermal annealed at 120 °C) and **2** (thermal annealed at 200 °C) were up to fifth and ninth order, respectively. The lattice d-spacing of **3** estimated from diffraction peaks was 26.44 Å, obviously shorter than compound **1** and **2**.

2.5. Thin Film Transistors Characterization

Thin film transistors with top-contact/bottom gate device configurations were fabricated with spin-coated thin films of **1**–**3** on octadecyltrichlorosine (OTS)-treated SiO_2/Si wafers. The gate is n-type heavily doped Si and the dielectric layer is a 300 nm thermally grown SiO_2. The Au source and drain electrodes were deposited through a shadow mask by vacuum evaporation, which gave a channel length of 31 μm and a width of 173 μm. All the devices were thermally annealed and measured under ambient conditions. The electron mobilities and threshold voltages were

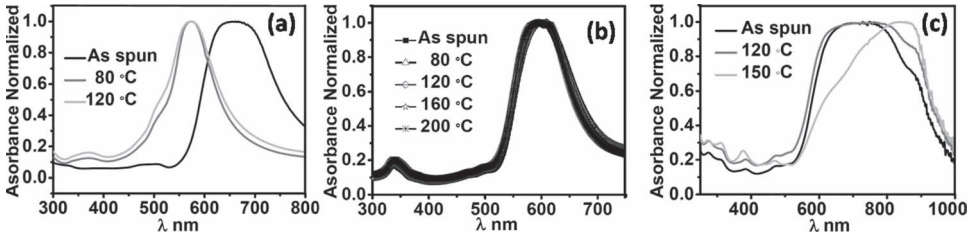

Figure 3. UV-vis absorption spectra of thin films before and after thermal annealing: a) **1**, b) **2**, and c) **3**.

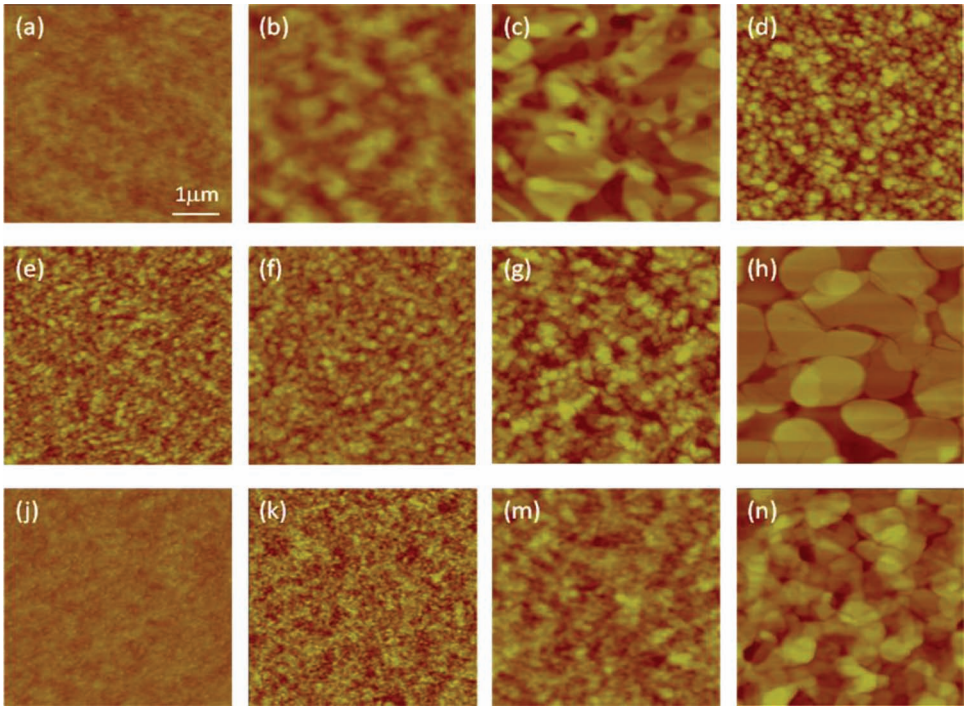

Figure 4. AFM images (5 mm × 5 mm) of thin films of **1**: a) As deposited, and annealed at b) 80 °C and c) 120 °C); **2**: d) as deposited, and annealed at e) 80 °C, f) 120 °C, g) 160 °C, and h) 200 °C; and **3**: j) as deposited, and annealed at k) 80 °C, m) 120 °C, and n) 150 °C.

calculated from the saturation regimes. The transistors performances were collected in the **Table 2** and the representative transfer and output plots were shown in **Figure 6**.

The as-deposited thin films of **1** exhibited no transistor performance, which is be due to the poor quality of the films, as proved by the XRD and AFM data. After thermal annealing, **1** displayed typical n-channel characteristics, and the highest electron mobility was 1.84×10^{-4} cm^2 V^{-1} s^{-1}. In contrast to **1**, the transistors based on as-deposited thin films of **2** showed high performance with electron mobilities up to 0.15 cm^2 V^{-1} s^{-1}. The electron mobility of **2** was slightly enhanced after thermal annealing at 120 and 160 °C, and a highest mobility of 0.22 cm^2 V^{-1} s^{-1} was observed, three orders of magnitude higher than that of **1**, when the thin films were thermal annealed at 120 °C. Further increasing the annealing temperature to 200 °C, no FET response was observed, ascribed to the increased grain boundary of the films. The transistors based on as-deposited thin films of **3** exhibited an electron mobility of 3.91×10^{-3} cm^2 V^{-1} s^{-1}. With thermal annealing, a mobility as high as 1.03×10^{-2} cm^2 V^{-1} s^{-1} was achieved. This value was two orders of magnitude higher than that of **1** and one order of magnitude lower than that of **2**.

2.6. Grazing-Incidence X-ray Diffraction (GIXD)

In order to further understand the effect of alkyl chain orientations on transistor performance, 2D GIXD was used to identify the molecular packing behavior in the thin films (**Figure 7**). All compounds displayed successive diffraction features in the q_z axis, indicating the conjugated cores were adopted lamellar packing model parallel to the surface with an edge-on orientation of the conjugated core. The thin films of **1** and **2** also contained a small populations of crystallites with tilted orientations as well as face-on domains, as inferred from arc shape reflections along q_z. The thin films of **3** exhibited stronger arc shape reflections along q_z compared with those of **1** and **2**, which indicated the thin films of **3** contained a larger fraction of face-on and tilted orientation domains.

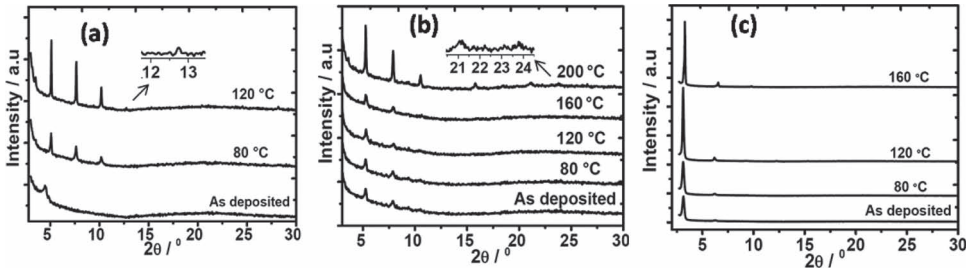

Figure 5. X-ray diffraction patterns of the spin-coated thin films of a) **1**, b) **2**, and c) **3** annealed at different temperatures.

Table 2. The performances of solution processed thin film transistors of OSCs **1**–**3**.

Compd	T [°C][a)]	μ_e [cm^2 V^{-1} s^{-1}]	$I_{on/off}$	V_{th} [V]
1	As deposited	NA	NA	NA
	120	(0.72–1.40)×10^{-4}	10–10^3	−10–5
2	As deposited	0.08–0.15	10^3–10^5	3–15
	120	0.14–0.22	10^4–10^5	3–13
3	As deposited	(1.93–3.91)×10^{-3}	10^2	−8-8
	150	(0.59–1.03)×10^{-2}	10^3	−8–6

[a)]Annealing temperatures given in this table were those that gave the best device performance.

The intermolecular π–π stacking is another important factor related to the FET performance. For the thin films of **1**, the d-spacing calculated from all the reflections were larger than 4 Å. Such large d-spacing indicated that no long-term π–π stacking transporting path existed in the thin films of **1**, which could explain the low devices performance of **1** even though the prepared thin films were smooth, continuous, and crystalline. The 2D GXRD patterns of compound **2** exhibited several short streak-like progressions, implying the high crystallinity of the films. The progressions were neither in q_z nor q_{xy} axis, and a d-spacing of 3.5 Å correlated with marked progression in Figure 7b, which arose from the π–π stacking diffraction, was observed, suggesting that the long axis of the conjugated backbone was tilted on the substrate. For the thin films of **3**, a π–π stacking reflection with d-spacing of 3.5 Å was clearly displayed along q_{xy} axis. The 2D GXRD results further confirmed the strong impact of alkyl chain orientation on molecular packing patterns and intermolecular interactions.

3. Conclusions

In summary, a series of dicyanomethylene-substituted 2,5-di(thiophen-2-yl)thieno[3,2-b]-thienoquinoid derivatives with 2-decyltetradecanyl substituted at the 2,2′- 3,3′- and 6,6′-positions (namely, compounds **1**–**3**) was strategically designed and successfully synthesized. The nearly identical CV scans and absorption spectra of these compounds in solution indicated that the orientation of alkyl substituents did not cause large distortions of the π-conjugated backbone and did not significant change the electron density distribution on the frontier molecular orbital; this was also supported by DFT calculations. However, compounds **1**–**3** adopted different molecular packing in the solid state which was evident from the XRD and thin film absorption spectra. Additionally, 2D GIXD spectra showed no long-term π–π stacking transporting paths existed in the thin films of **1**, while π–π stackings with d-spacing of 3.5 Å were observed for the thin films of **2** and **3**. All compounds exhibited ambient stable TFT performance. The highest electron mobility of 0.22 cm^2 V^{-1} s^{-1} was recorded for thin films of **2**, which was one and three orders of magnitude higher than those of **3** and **1**, respectively. The wide variation of FET performances is ascribed to the different molecular packing patterns in the thin film and different film morphology of **1**–**3** which is caused by the alkyl chain orientation. These results indicate that modifying the side alkyl chain orientation is an important method, likely to receive more attention for the rational design of high performance OSCs.

4. Experimental Section

Synthesis of Compound ***1***: Malononitrile (168 mg, 2.54 mmol) was added to an ice-salt cooled suspension of sodium hydride (122 mg, 5.07 mmol) in 1,2-dimethoxyethane (20 mL) under a nitrogen stream. The mixture was stirred at room temperature for another 20 min. Then, **4** (0.72 g, 0.63 mmol) and tetrakis(triphenylphosphine) palladium (147 mg, 0.13 mmol) were added, the solution was heated under reflux for 4 h. The resulting solution was treated with saturated bromine water (20 mL) and the precipitation was filtered. After washed with water and dried under vacuum, the crude product purified by flash chromatographyon silica. Light petroleum-dichloromethane (ratio 1:1) eluted compound **1** (0.32 g, 45.7%). ^{1}H NMR (300 MHz, $CDCl_3$, δ): 0.88 (t, J = 6.6Hz, 12H; CH_3), 1.25 (Br, 80H; CH_2), 1.79 (Br, 2H; CH), 2.83 (d, J = 5.1Hz, 4H; CH_2), 7.13 (Br, 2H; Ar H), 7.27 (Br, 2H; Ar H); ^{13}C NMR (100 MHz, $CDCl_3$, δ): 14. 11, 22. 88, 26. 08, 29. 35, 29. 61, 29. 65, 29. 83, 29. 94, 31.

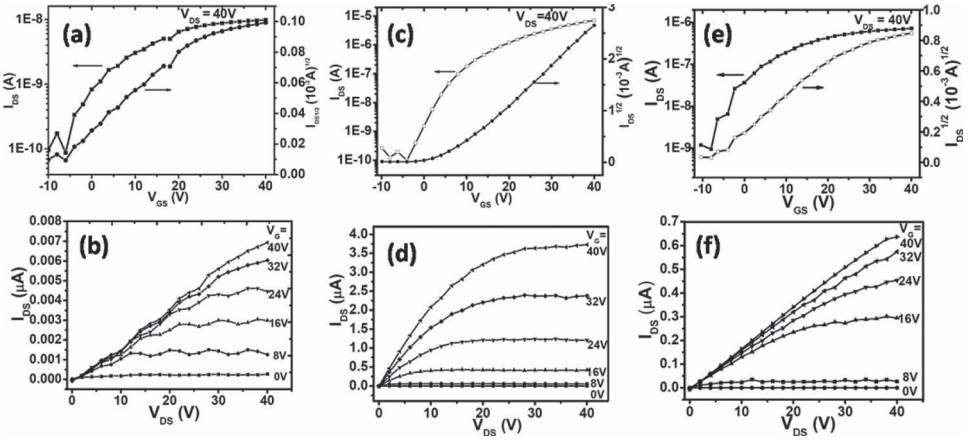

Figure 6. Solution processed thin film transistor characteristics: a) transfer and b) output curves of **1**, c) transfer and d) output curves of **2**, e) transfer and f) output curves of **3**.

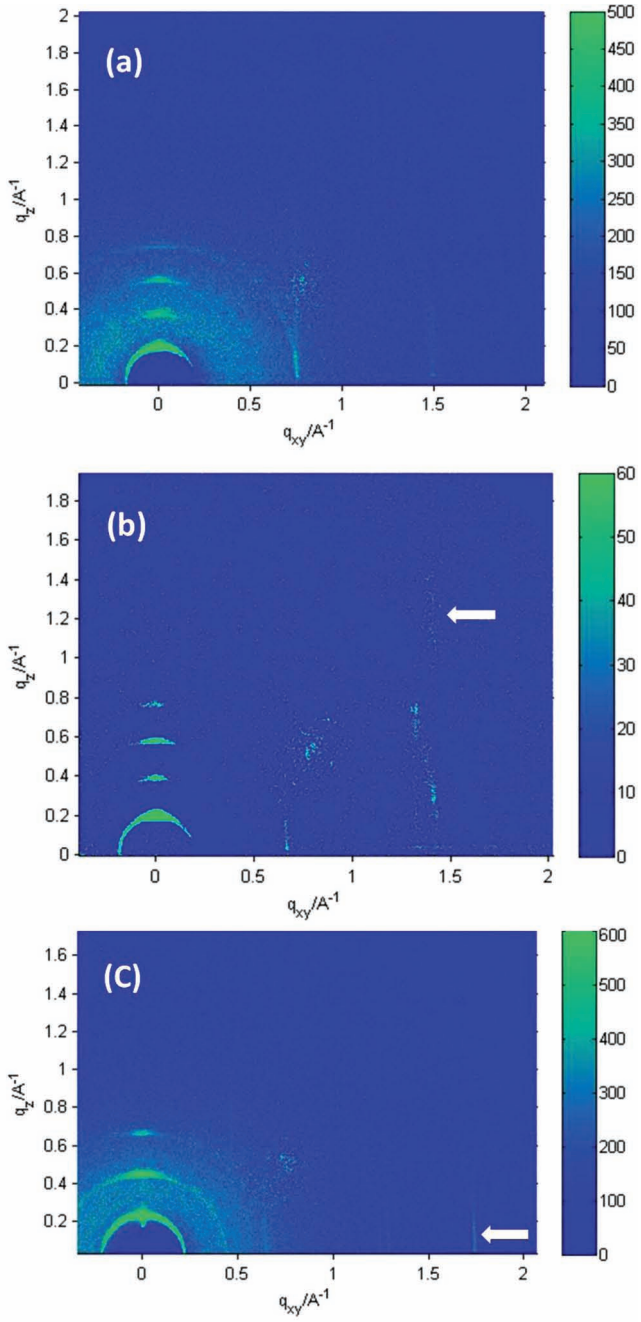

Figure 7. Two-dimensional grazing-incidence X-ray diffraction (2D-GIXD) of thin films. a) **1** (annealed at 120 °C); b) **2** (annealed at 200 °C); and c) **3** (annealed at 150 °C)

91, 32. 63, 34. 34, 38. 06, 113. 88, 115. 33, 119. 73, 138. 05, 145. 07, 146. 67, 148. 09, 151. 86, 166. 99; MS (MALDI-TOF) *m/z*: 1103.7 (M^++H); HRMS (MALDI, *m/z*) [M+H]$^+$ calcd for $C_{68}H_{103}N_4S_4$, 1103.7067; found, 1103.7060. Anal. Calcd for $C_{68}H_{102}N_4S_4$: C, 73.99; H, 9.31; N, 5.08%; Found: C, 73.80; H, 9.29; N, 4.97%.

Synthesis of Compound **2**: **2** was prepared according to the procedure for the synthesis of compound **1** in 45.0% yield. ^{1}H NMR (300 MHz, $CDCl_3$, δ): 0.88 (t, J = 6.6Hz, 12H; CH_3), 1.26 (Br, 80H; CH_2), 1.84 (Br, 2H; CH), 2.75 (d, J = 6.9Hz, 4H; CH_2), 7.08 (s, 2H; Ar H), 7.20 (s, 2H; Ar H); ^{13}C NMR (100 MHz, $CDCl_3$, δ): 14.12, 22.69, 26.23, 29.36, 29.64, 29.92, 31.91, 33.28, 36.31, 37.45, 113.48, 114.33, 121.34, 132.89, 136.30, 145.31, 152.33, 155.64, 167.11; MS (MALDI-TOF) *m/z*: 1103.7 (M^++H); HRMS (MALDI, *m/z*) [M+H]$^+$ calcd for $C_{68}H_{103}N_4S_4$, 1103.7074; found 1103.7060. Anal. Calcd for $C_{68}H_{102}N_4S_4$: C, 73.99; H, 9.31; N, 5.08%; Found: C, 73.80; H, 9.59; N, 4.97%.

Synthesis of Compound **3**: **3** was prepared according to the procedure for the synthesis of compound **1** in 46.6% yield. ^{1}H NMR (300 MHz, $CDCl_3$, δ): 0.88 (t, J = 6.6Hz, 12H; CH_3), 1.24 (Br, 80H, CH_2), 1.93 (Br, 2H; CH), 2.79 (d, J = 7.5, 4H; CH_2), 7.29 (d, J = 5.4, 2H; Ar H), 7.56 (d, J = 5.4, 2H; Ar H); ^{13}C NMR (100 MHz,$CDCl_3$, δ): 14. 10, 22. 67, 26. 21, 29. 34, 29. 62, 29. 68, 29. 90, 31. 90, 33. 26, 36. 29, 37. 43, 113. 47, 114. 31, 121. 39, 132. 87, 136. 28, 145. 29, 152. 27, 155. 63, 167. 10; MS (MALDI-TOF) *m/z*: 1103.7(M^++H); HRMS (MALDI, *m/z*) [M+H]$^+$ calcd for $C_{68}H_{103}S_4N_4$, 1103.7066; found 1103.7060. Anal. Calcd for $C_{68}H_{102}N_4S_4$: C, 73.99; H, 9.31; N, 5.08%; Found: C, 73.85; H, 9.14; N, 4.78%.

Supporting Information

Supporting Information is available from the Wiley Online Library or from the author.

Acknowledgements

This work was supported by National Natural Sciences Foundation of China (21190031, 51273212) and National Basic Research Program of China (2011CB808405). The authors thank beamline BL14B1 (Shanghai Synchrotron Radiation Facility) for providing the beam time.

Received: September 21, 2012
Published online: December 2, 2012

[1] a) S. R. Forrest, *Nature* **2004**, *428*, 911; b) H. E. Huitema, G. H. Gelinck, J. B. van der Putten, K. E. Kuijk, C. M. Hart, E. Cantatore, P. T. Herwig, A. J. van Breemen, D. M. de Leeuw, *Nature* **2001**, *414*, 599; c) D. Voss, *Nature* **2000**, *407*, 442; d) P. Andersson, R. Forchheimer, P. Tehrani, M. Berggren, *Adv. Funct. Mater.* **2007**, *17*, 3074; e) B. K. Crone, A. Dodabalapur, R. Sarpeshkar, A. Gelperin, H. E. Katz, Z. Bao, *J. Appl. Phys.* **2002**, *91*, 10140; f) M. A. McCarthy, B. Liu, E. P. Donoghue, I. Kravchenko, D. Y. Kim, F. So, A. G. Rinzler, *Science* **2011**, *332*, 570; g) J. Sun, B. Zhang, H. E. Katz, *Adv. Funct. Mater.* **2011**, *21*, 29; h) G. Gelinck, P. Heremans, K. Nomoto, T. D. Anthopoulos, *Adv. Mater.* **2010**, *22*, 3778; i) T. Someya, A. Dodabalapur, J. Huang, K. C. See, H. E. Katz, *Adv. Mater.* **2010**, *22*, 3799.

[2] H. Sirringhaus, P. J. Brown, R. H. Friend, M. M. Nielsen, K. Bechgaard, B. M. W. Langeveld-Voss, A. J. H. Spiering, R. A. J. Janssen, E. W. Meijer, P. Herwig, D. M. de Leeuw, *Nature* **1999**, *401*, 685.

[3] M. M. Payne, S. R. Parkin, J. E. Anthony, C. C. Kuo, T. N. Jackson, *J. Am. Chem. Soc.* **2005**, *127*, 4986.

[4] a) X. Zhang, L. J. Richter, D. M. DeLongchamp, R. J. Kline, M. R. Hammond, I. McCulloch, M. Heeney, R. S. Ashraf, J. N. Smith, T. D. Anthopoulos, B. Schroeder, Y. H. Geerts, D. A. Fischer, M. F. Toney, *J. Am. Chem. Soc.* **2011**, *133*, 15073; b) I. McCulloch, M. Heeney, M. L. Chabinyc, D. DeLongchamp, R. J. Kline, M. Coelle, W. Duffy, D. Fischer, D. Gundlach, B. Hamadani, R. Hamilton, L. Richter, A. Salleo, M. Shkunov, D. Sporrowe, S. Tierney, W. Zhong, *Adv. Mater.* **2009**, *21*, 1091; c) J. A. Lim, H. S. Lee, W. H. Lee, K. Cho, *Adv. Funct. Mater.* **2009**, *19*, 1515.

[5] a) K. P. Goetz, Z. Li, J. W. Ward, C. Bougher, J. Rivnay, J. Smith, B. R. Conrad, S. R. Parkin, T. D. Anthopoulos, A. Salleo, J. E. Anthony, O. D. Jurchescu, *Adv. Mater.* **2011**, *23*, 3698;

b) A. N. Sokolov, S. Atahan-Evrenk, R. Mondal, H. B. Akkerman, R. S. Sanchez-Carrera, S. Granados-Focil, J. Schrier, S. C. Mannsfeld, A. P. Zoombelt, Z. Bao, A. Aspuru-Guzik, *Nature* **2011**, *2*, 437; c) K. Niimi, S. Shinamura, I. Osaka, E. Miyazaki, K. Takimiya, *J. Am. Chem. Soc.* **2011**, *133*, 8732; d) M. L. Tang, T. Okamoto, Z. Bao, *J. Am. Chem. Soc.* **2006**, *128*, 16002; e) K. Takimiya, S. Shinamura, I. Osaka, E. Miyazaki, *Adv. Mater.* **2011**, *23*, 4347; f) J. Youn, P. Y. Huang, Y. W. Huang, M. C. Chen, Y. J. Lin, H. Huang, R. P. Ortiz, C. Stern, M. C. Chung, C. Y. Feng, L. H. Chen, A. Facchetti, T. J. Marks, *Adv. Funct. Mater.* **2012**, *22*, 48.

[6] a) K. Takimiya, Y. Kunugi, Y. Konda, H. Ebata, Y. Toyoshima, T. Otsubo, *J. Am. Chem. Soc.* **2006**, *128*, 3044; b) Y. Y. Liu, C. L. Song, W. J. Zeng, K. G. Zhou, Z. F. Shi, C. B. Ma, F. Yang, H. L. Zhang, X. Gong, *J. Am. Chem. Soc.* **2010**, *132*, 16349; c) J. S. Ha, K. H. Kim, D. H. Choi, *J. Am. Chem. Soc.* **2011**, *133*, 10364.

[7] a) S. Shinamura, I. Osaka, E. Miyazaki, A. Nakao, M. Yamagishi, J. Takeya, K. Takimiya, *J. Am. Chem. Soc.* **2011**, *133*, 5024; b) L. Ying, B. B. Hsu, H. Zhan, G. C. Welch, P. Zalar, L. A. Perez, E. J. Kramer, T. Q. Nguyen, A. J. Heeger, W. Y. Wong, G. C. Bazan, *J. Am. Chem. Soc.* **2011**, *133*, 18538; c) M. L. Tang, A. D. Reichardt, T. Okamoto, N. Miyaki, Z. A. Bao, *Adv. Funct. Mater.* **2008**, *18*, 1579.

[8] P. Gao, D. Beckmann, H. N. Tsao, X. L. Feng, V. Enkelmann, M. Baumgarten, W. Pisula, K. Mullen, *Adv. Mater.* **2009**, *21*, 213.

[9] a) T. Izawa, H. Mori, Y. Shinmura, M. Iwatani, E. Miyazaki, K. Takimiya, H. W. Hung, M. Yahiro, C. Adachi, *Chem. Lett.* **2009**, *38*, 420; b) T. Izawa, E. Miyazaki, K. Takimiya, *Chem. Mater.* **2009**, *21*, 903.

[10] a) R. J. Kline, D. M. DeLongchamp, D. A. Fischer, E. K. Lin, L. J. Richter, M. L. Chabinyc, M. F. Toney, M. Heeney, I. McCulloch, *Macromolecules* **2007**, *40*, 7960; b) B. S. Ong, Y. Wu, Y. Li, P. Liu, H. Pan, *Chemistry* **2008**, *14*, 4766.

[11] a) M. Halik, H. Klauk, U. Zschieschang, G. Schmid, S. Ponomarenko, S. Kirchmeyer, W. Weber, *Adv. Mater.* **2003**, *15*, 917; b) Y. D. Park, D. H. Kim, Y. Jang, J. H. Cho, M. Hwang, H. S. Lee, J. A. Lim, K. Cho, *Org. Electron.* **2006**, *7*, 514; c) A. Babel, S. A. Jenekhe, *Synth. Met.* **2005**, *148*, 169.

[12] H. N. Tsao, D. M. Cho, I. Park, M. R. Hansen, A. Mavrinskiy, Y. D. Yoon, R. Graf, W. Pisula, H. W. Spiess, K. Mullen, *J. Am. Chem. Soc.* **2011**, *133*, 2605.

[13] a) H. Bronstein, D. S. Leem, R. Hamilton, P. Woebkenberg, S. King, W. M. Zhang, R. S. Ashraf, M. Heeney, T. D. Anthopoulos, J. de Mello, I. McCulloch, *Macromolecules* **2011**, *44*, 6649; b) I. McCulloch, M. Heeney, C. Bailey, K. Genevicius, I. Macdonald, M. Shkunov, D. Sparrowe, S. Tierney, R. Wagner, W. Zhang, M. L. Chabinyc, R. J. Kline, M. D. McGehee, M. F. Toney, *Nat. Mater.* **2006**, *5*, 328.

[14] a) J. Mei, D. H. Kim, A. L. Ayzner, M. F. Toney, Z. Bao, *J. Am. Chem. Soc.* **2011**, *133*, 20130; b) A. Kreyes, S. Ellinger, K. Landfester, M. Defaux, D. A. Ivanov, A. Elschner, T. Meyer-Friedrichsen, U. Ziener, *Chem. Mater.* **2010**, *22*, 2079; c) Z. Li, Y. G. Zhang, S. W. Tsang, X. M. Du, J. Y. Zhou, Y. Tao, J. F. Ding, *J. Phys. Chem. C* **2011**, *115*, 18002.

[15] a) M. J. Panzer, C. D. Frisbie, *J. Am. Chem. Soc* **2007**, *129*, 6599; b) H. Pan, Y. Wu, Y. Li, P. Liu, B. S. Ong, S. Zhu, G. Xu, *Adv. Funct. Mater.* **2007**, *17*, 3574.

[16] a) J. Liu, R. Zhang, G. Sauve, T. Kowalewski, R. D. McCullough, *J. Am. Chem. Soc.* **2008**, *130*, 13167; b) J. Kumagai, K. Hirano, T. Satoh, S. Seki, M. Miura, *J. Phs. Chem. B* **2011**, *115*, 8446; c) X. Guo, R. P. Ortiz, Y. Zheng, M. G. Kim, S. Zhang, Y. Hu, G. Lu, A. Facchetti, T. J. Marks, *J. Am. Chem. Soc.* **2011**, *133*, 13685.

[17] a) S. Subramanian, S. K. Park, S. R. Parkin, V. Podzorov, T. N. Jackson, J. E. Anthony, *J. Am. Chem. Soc.* **2008**, *130*, 2706; b) H. Minemawari, T. Yamada, H. Matsui, J. Tsutsumi, S. Haas, R. Chiba, R. Kumai, T. Hasegawa, *Nature* **2011**, *475*, 364; c) H. Bronstein, Z. Chen, R. S. Ashraf, W. Zhang, J. Du, J. R. Durrant, P. S. Tuladhar, K. Song, S. E. Watkins, Y. Geerts, M. M. Wienk, R. A. Janssen, T. Anthopoulos, H. Sirringhaus, M. Heeney, I. McCulloch, *J. Am. Chem. Soc.* **2011**, *133*, 3272; d) J. S. Lee, S. K. Son, S. Song, H. Kim, D. R. Lee, K. Kim, M. J. Ko, D. H. Choi, B. Kim, J. H. Cho, *Chem. Mater.* **2012**, *24*, 1316; e) H. Chen, Y. Guo, G. Yu, Y. Zhao, J. Zhang, D. Gao, H. Liu, Y. Liu, *Adv. Mater.* **2012**, *24*, 4618.

[18] a) J. H. Oh, H. W. Lee, S. Mannsfeld, R. M. Stoltenberg, E. Jung, Y. W. Jin, J. M. Kim, J. B. Yoo, Z. Bao, *Proc. Natl. Acad. Sci. USA* **2009**, *106*, 6065; b) H. Yan, Z. Chen, Y. Zheng, C. Newman, J. R. Quinn, F. Dotz, M. Kastler, A. Facchetti, *Nature* **2009**, *457*, 679; c) X. Gao, C. A. Di, Y. Hu, X. Yang, H. Fan, F. Zhang, Y. Liu, H. Li, D. Zhu, *J. Am. Chem. Soc.* **2010**, *132*, 3697; d) H. Usta, A. Facchetti, T. J. Marks, *J. Am. Chem. Soc.* **2008**, *130*, 8580; e) Z. Liang, Q. Tang, J. Xu, Q. Miao, *Adv. Mater.* **2011**, *23*, 1535; f) H. Usta, A. Facchetti, T. J. Marks, *Acc. Chem. Res* **2011**, *44*, 501; g) B. J. Jung, N. J. Tremblay, M. L. Yeh, H. E. Katz, *Chem. Mater.* **2011**, *23*, 568; h) Y. Wen, Y. Liu, *Adv. Mater.* **2010**, *22*, 1331; i) S. Kola, J. Sinha, H. E. Katz, *J. Polym. Sci., Part B: Polym. Phys.* **2012**, *50*, 1090.

[19] a) E. J. Meijer, D. M. de Leeuw, S. Setayesh, E. van Veenendaal, B. H. Huisman, P. W. Blom, J. C. Hummelen, U. Scherf, J. Kadam, T. M. Klapwijk, *Nat. Mater.* **2003**, *2*, 678; b) H. Klauk, U. Zschieschang, J. Pflaum, M. Halik, *Nature* **2007**, *445*, 745.

[20] a) J. Ferraris, V. Walatka, Perlstei. Jh, D. O. Cowan, *J. Am. Chem. Soc.* **1973**, *95*, 948; b) N. Martin, P. de Miguel, C. Seoane, A. Albert, F. H. Cano, *J. Mater. Chem.* **1997**, *7*, 25; c) S. Yoshida, M. Fujii, Y. Aso, T. Otsubo, F. Ogura, *J. Org. Chem.* **1994**, *59*, 3077; d) K. Yui, Y. Aso, T. Otsubo, F. Ogura, *J. Chem. Soc., Chem. Commun.* **1987**, 1816.

[21] K. Yui, H. Ishida, Y. Aso, T. Otsubo, F. Ogura, A. Kawamoto, J. Tanaka, *Bull. Chem. Soc. Jpn.* **1989**, *62*, 1547.

[22] a) S. Handa, E. Miyazaki, K. Takimiya, *Chem. Commun.* **2009**, 3919; b) T. Kashiki, E. Miyazaki, K. Takimiya, *Chem. Lett.* **2009**, *38*, 568; c) Y. Kunugi, K. Takimiya, Y. Toyoshima, K. Yamashita, Y. Aso, T. Otsubo, *J. Mater. Chem.* **2004**, *14*, 1367; d) E. Menard, V. Podzorov, S. H. Hur, A. Gaur, M. E. Gershenson, J. A. Rogers, *Adv. Mater.* **2004**, *16*, 2097; e) J. C. Ribierre, T. Fujihara, S. Watanabe, M. Matsumoto, T. Muto, A. Nakao, T. Aoyama, *Adv. Mater.* **2010**, *22*, 1722; f) Y. Suzuki, M. Shimawaki, E. Miyazaki, I. Osaka, K. Takimiya, *Chem. Mater.* **2011**, *23*, 795; g) M. Yamagishi, Y. Tominari, T. Uemura, J. Takeya, *Appl. Phys. Lett.* **2009**, 94; h) J. G. Laquindanum, H. E. Katz, A. Dodabalapur, A. J. Lovinger, *J. Am. Chem. Soc.* **1996**, *118*, 11331; i) A. R. Brown, D. M. Deleeuw, E. J. Lous, E. E. Havinga, *Synth. Met.* **1994**, *66*, 257; j) H. Zhong, J. Smith, S. Rossbauer, A. J. White, T. D. Anthopoulos, M. Heeney, *Adv. Mater.* **2012**, *24*, 3205.

[23] Y. Suzuki, E. Miyazaki, K. Takimiya, *J. Am. Chem. Soc.* **2010**, *132*, 10453.

[24] a) T. M. Pappenfus, R. J. Chesterfield, C. D. Frisbie, K. R. Mann, J. Casado, J. D. Raff, L. L. Miller, *J. Am. Chem. Soc.* **2002**, *124*, 4184; b) D. E. Janzen, M. W. Burand, P. C. Ewbank, T. M. Pappenfus, H. Higuchi, D. A. da Silva Filho, V. G. Young, J. L. Bredas, K. R. Mann, *J. Am. Chem. Soc.* **2004**, *126*, 15295.

[25] R. J. Chesterfield, C. R. Newman, T. M. Pappenfus, P. C. Ewbank, M. H. Haukaas, K. R. Mann, L. L. Miller, C. D. Frisbie, *Adv. Mater.* **2003**, *15*, 1278.

[26] a) S. Handa, E. Miyazaki, K. Takimiya, Y. Kunugi, *J. Am. Chem. Soc.* **2007**, *129*, 11684; b) Y. Qiao, Y. Guo, C. Yu, F. Zhang, W. Xu, Y. Liu, D. Zhu, *J. Am. Chem. Soc.* **2012**, *134*, 4084.

[27] Q. H. Wu, R. J. Li, W. Hong, H. X. Li, X. K. Gao, D. B. Zhu, *Chem. Mater.* **2011**, *23*, 3138.

[28] a) D. M. de Leeuw, M. M. J. Simenon, A. R. Brown, R. E. F. Einerhand, *Synth. Met.* **1997**, *87*, 53; b) B. A. Jones, A. Facchetti, M. R. Wasielewski, T. J. Marks, *J. Am. Chem. Soc.* **2007**, *129*, 15259.

[29] A. Mishra, R. K. Behera, P. K. Behera, B. K. Mishra, G. B. Behera, *Chem. Rev.* **2000**, *100*, 1973.